International Journal of Power Electronics and Drive Systems (IJPEDS)
Vol. 15, No. 3, September 2024, pp. 1838~1850
ISSN: 2088-8694, DOI: 10.11591/ijpeds.v15.i3.pp1838-1850

A nonlinear control in αβ reference frame for single-stage three-phase grid-connected photovoltaic systems with an LCL-filter

Zakariae El Madani, Abdelhafid Yahya, Zakaria El Malki
Department of Electrical Engineering, Higher School of Technology, Moulay Ismail University, Meknes, Morocco

Article Info

Article history:

Received Oct 23, 2023
Revised Mar 14, 2024
Accepted Mar 21, 2024

Keywords:

Grid-connected PV system
LCL-filter
MPPT
Nonlinear control
Single-stage
αβ reference frame

ABSTRACT

This paper presents a nonlinear control in the stationary αβ reference frame for single-stage three-phase grid-connected photovoltaic systems. The system under study consists of a photovoltaic generator (PVG), a three-phase inverter, and an LCL-filter on the grid side. The main control objectives are to extract the maximum power from the PVG and deliver that power into the grid with high-quality power i.e. unity power factor (UPF). In order to achieve these objectives, a nonlinear controller is designed by using backstepping technique. The performance of this controller is evaluated under standard and variable atmospheric conditions. Simulation results demonstrate that the proposed controller has successfully met all the specified objectives. This study highlights the potential of using the nonlinear control based on backstepping technique in photovoltaic systems with LCL-filters. The modeling and simulation of the complete system are carried out using MATLAB/Simulink environment.

Corresponding Author:

Zakariae El Madani
Department of Electrical Engineering, Higher School of Technology, Moulay Ismail University
Marjane 2, Meknes 50050, Morocco
Email: zakariae.elmadani@gmail.com

1. INTRODUCTION

Recently, renewable energy sources such as solar, wind, geothermal, and hydro have gained more attention as alternative means of generating electricity. Due to their immense potential, these energy sources are being increasingly utilized in industrial and building sectors [1]. Solar energy, especially photovoltaic solar energy is currently considered one of the most promising clean energy sources due to its wide availability and ease of use.

In a grid-connected PV system, the power extracted from photovoltaic arrays can be injected into the utility grid. To enhance the efficiency of PV system, it is necessary to operate the PVG at its maximum power point (MMP). This can be achieved through the implementation of a maximum power point tracking (MPPT) algorithm. Several MPPT algorithms have been proposed for this purpose [2]-[10], the most popular one being the perturb and observe algorithm.

The energy transfer between the PVG and the utility grid is realized by mean of power converters. In this context, two main topologies have been distinguished [11], [12]. The first topology is the double-stage PV systems, where the grid is connected to the PVG through a DC/DC converter, acting as a maximum power point (MPP) tracker, and a DC/AC converter for power factor correction (PFC) [13]-[16]. The second topology, known as single-stage PV systems, where the utility grid is directly tied to the PVG through a DC/AC converter in order to achieve both MPPT and PFC requirements [11], [12]-[22].

The grid-connected photovoltaic systems adopt single-stage power conversion to minimize circuit complexity, size, and cost [12]. In this topology, the conventional voltage-source inverter (VSI) is used to

process power and inject a sinusoidal current into the grid. An L-filter is commonly utilized to reduce current harmonics at the inverter output, a solution widely adopted in various studies [12], [17]-[21]. However, in this research, we implement an LCL-filter to mitigate current harmonics. The primary reason for selecting this filter lies in its several advantages over the L-filter, including superior attenuation capability, smaller inductances, and the ability to operate at lower switching frequencies [23]-[29]. To date, only a few control schemes have been reported for single-stage three-phase grid-connected PV systems with an LCL-filter that aim to meet MPPT and UPF requirements. An adaptive control scheme for three-phase grid-connected inverters in photovoltaic power generation is presented to control the current injected into the grid [30]. An output feedback MRAC scheme for three-phase grid-connected inverters in photovoltaic power generation systems [31].

The primary objective of this research is to design a nonlinear controller using the nonlinear model of a single-stage three-phase grid-connected PV system with an LCL-filter. The controller aims to achieve the following key objectives: i) Ensuring the PV system operates at its MPP, even under varying climatic conditions and ii) Ensuring UPF on the grid side. The rest of this paper is organized as follows: i) Section 2 provides a description and mathematical modeling of the proposed system; ii) Section 3 details the design of the controller in the stationary αβ reference frame; and iv) Section 4 displays simulation results in order to validate the desired performance.

2. POWER SYSTEM CONFIGURATION AND MODELING

2.1. PV system configuration

The PV modules used in this study are of type sharp NU-183E1. Our PV generator is made up of 16 parallel strings, with each string comprising 34 series-connected modules. The specific PV module parameters are detailed in Table 1. Figure 1 and Figure 2 illustrate the power-voltage(P-V) characteristics curves of this generator under different solar irradiation and temperature conditions, respectively. Table 2 presents the maximum power that this generator can deliver under certain solar irradiation conditions, while Table 3 shows the maximum power it can deliver under specific temperature conditions. These tables are utilized in section 4 to evaluate the performance of the complete system.

Table 1. NU-183E1 parameters under standard test conditions (STC)

Parameter	Value
Maximum power (W)	183
Current at maximum power (A)	7.66
Voltage at maximum power (V)	23.9
Short-circuit current (A)	8.48
Open-circuit voltage (V)	30.1
Number of series cells	48
Number of parallel cells	1

Table 2. Maximum power point (MPP) of PVG under different irradiation values and standard temperature T = 25 °C (see Figure 1)

Irradiation (W/m^2)	MPP	Value (W)
1000	MPP1	99608
800	MPP2	79395
600	MPP3	58979
400	MPP4	38515

Table 3. Maximum power point (MPP) of PVG under different temperature values and standard irradiation E = 1000 W/m^2 (see Figure 2)

Temperature (°C)	MPP	Value (W)
15	MPP5	104279
25	MPP6	99608
35	MPP7	94954
45	MPP8	90322

2.2. Power system modeling

The proposed grid-connected PV system is depicted in Figure 3, while the system parameters are presented in Table 4. The VSI is comprised of three legs, each having two switches that are controlled by a sinusoidal pulse width modulation (SPWM) signals. The semiconductor switches are symbolized as switches S_a, S_b and S_c. The status of each switch is denoted by "0" for the open state and "1" for the closed state. The complementary switches S_a, S_b and S_c operate opposite $\bar{S}_a$, $\bar{S}_b$ and $\bar{S}_c$. The LCL-filter consists of an inductor L_f on the inverter's side, a capacitor C_f, an inductor L_g on the grid side, and the equivalent resistance R_f, R_g of the inductor L_f and L_g respectively. The grid voltages e_{ga},e_{gb} and e_{gc} form a balanced three-phase system.

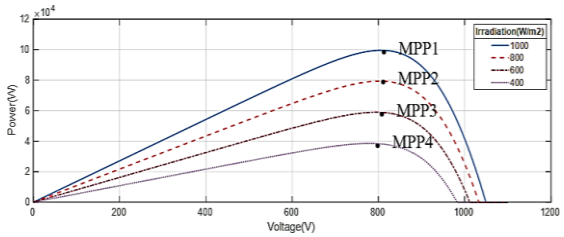

Figure 1. P-V characteristics of PVG under different irradiation values and standard temperature T= 25 °C

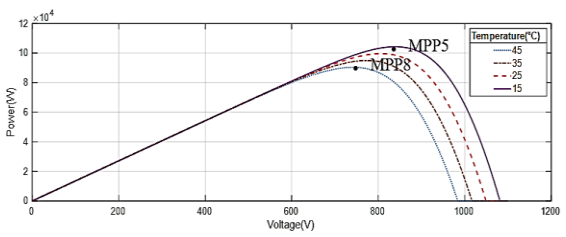

Figure 2. P-V characteristics of PVG under different temperature values and standard irradiation E=1000 W/m^2

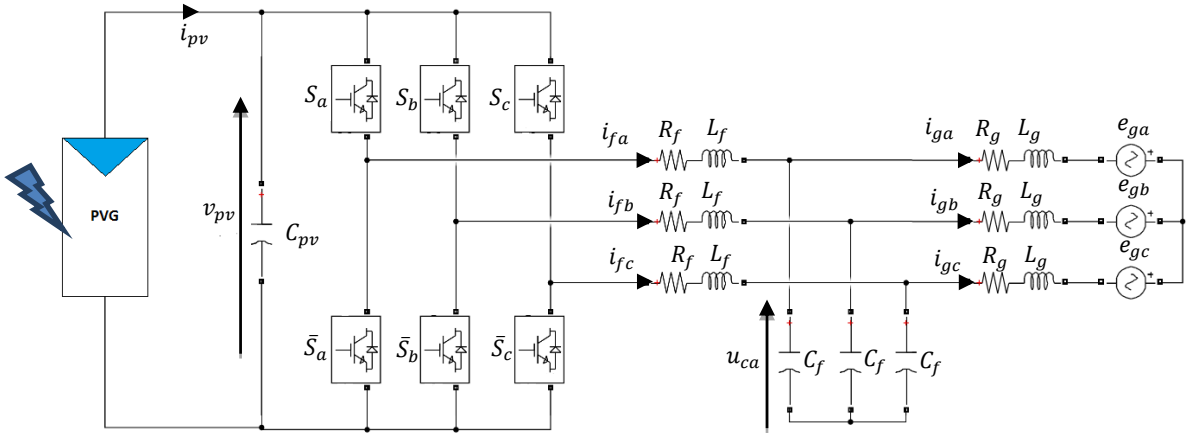

Figure 3. Single-stage three-phase grid-connected PV system with LCL-filter

Table 4. System parameter description

Parameter	Symbole	Value
Grid voltage	e_g	220 V
Grid frequency	f	50 Hz
VSI side inductor	L_f	1.2 mH
Grid side inductor	L_g	1.2 mH
Resistance of inductor L_f	R_f	0.2 Ω
Resistance of inductor L_g	R_g	0.2 Ω
Filter capacitor	C_f	6 µF
DC link capacitor	C_{pv}	3.300 mF
Switching frequency	f_s	5 kHz

Applying Kirchhoff's laws to the system shown in Figure 3, the resulting switched model in the stationary ABC-frame is as:

$$L_g.\frac{d}{dt}\begin{bmatrix} i_{ga} \\ i_{gb} \\ i_{gc} \end{bmatrix} = -R_g \begin{bmatrix} i_{ga} \\ i_{gb} \\ i_{gc} \end{bmatrix} + \begin{bmatrix} u_{ca} \\ u_{cb} \\ u_{cc} \end{bmatrix} - \begin{bmatrix} e_{ga} \\ e_{gb} \\ e_{gc} \end{bmatrix} \quad (1)$$

$$C_f.\frac{d}{dt}\begin{bmatrix} u_{ca} \\ u_{cb} \\ u_{cc} \end{bmatrix} = \begin{bmatrix} i_{fa} \\ i_{fb} \\ i_{fc} \end{bmatrix} - \begin{bmatrix} i_{ga} \\ i_{gb} \\ i_{gc} \end{bmatrix} \quad (2)$$

$$L_f.\frac{d}{dt}\begin{bmatrix} i_{fa} \\ i_{fb} \\ i_{fc} \end{bmatrix} = -R_f \begin{bmatrix} i_{fa} \\ i_{fb} \\ i_{fc} \end{bmatrix} + \frac{v_{pv}}{3}\begin{bmatrix} 2 & -1 & -1 \\ -1 & 2 & -1 \\ -1 & -1 & 2 \end{bmatrix}\begin{bmatrix} S_a \\ S_b \\ S_c \end{bmatrix} - \begin{bmatrix} u_{ca} \\ u_{cb} \\ u_{cc} \end{bmatrix} \quad (3)$$

$$C_{pv}.\frac{dv_{pv}}{dt} = i_{pv} - [S_a \quad S_b \quad S_c]\begin{bmatrix} i_{fa} \\ i_{fb} \\ i_{fc} \end{bmatrix} \tag{4}$$

For the sake of control design, it is more practical to work with the following averaged model, derived by averaging model (1)-(4) over a switching period Ts [32].

$$L_g.\frac{d}{dt}\begin{bmatrix} I_{ga} \\ I_{gb} \\ I_{gc} \end{bmatrix} = -R_g\begin{bmatrix} I_{ga} \\ I_{gb} \\ I_{gc} \end{bmatrix} + \begin{bmatrix} U_{ca} \\ U_{cb} \\ U_{cc} \end{bmatrix} - \begin{bmatrix} E_{ga} \\ E_{gb} \\ E_{gc} \end{bmatrix} \tag{5}$$

$$C_f.\frac{d}{dt}\begin{bmatrix} U_{ca} \\ U_{cb} \\ U_{cc} \end{bmatrix} = \begin{bmatrix} I_{fa} \\ I_{fb} \\ I_{fc} \end{bmatrix} - \begin{bmatrix} I_{ga} \\ I_{gb} \\ I_{gc} \end{bmatrix} \tag{6}$$

$$L_f.\frac{d}{dt}\begin{bmatrix} I_{fa} \\ I_{fb} \\ I_{fc} \end{bmatrix} = -R_f\begin{bmatrix} I_{fa} \\ I_{fb} \\ I_{fc} \end{bmatrix} + \frac{V_{pv}}{3}\begin{bmatrix} 2 & -1 & -1 \\ -1 & 2 & -1 \\ -1 & -1 & 2 \end{bmatrix}\begin{bmatrix} \mu_a \\ \mu_b \\ \mu_c \end{bmatrix} - \begin{bmatrix} U_{ca} \\ U_{cb} \\ U_{cc} \end{bmatrix} \tag{7}$$

$$C_{pv}.\frac{dV_{pv}}{dt} = I_{pv} - [\mu_a \quad \mu_b \quad \mu_c]\begin{bmatrix} I_{fa} \\ I_{fb} \\ I_{fc} \end{bmatrix} \tag{8}$$

where $I_{fa,b,c}$, $I_{ga,b,c}$, $U_{ca,b,c}$, V_{pv}, and $\mu_{a,b,c}$ are the average values over Ts of the signals $i_{fa,b,c}$, $i_{ga,b,c}$, $u_{ca,b,c}$, v_{pv}, and $s_{a,b,c}$ respectively.

To facilitate the design of the controller, the αβ transformation has been adopted in this paper. Applying Clarke's transformation to (5)-(8) [33], the model of the single-stage three-phase grid-connected PV system in the stationary αβ reference frame is as:

$$L_g.\dot{I}_{g\alpha} = -R_g.I_{g\alpha} + U_{c\alpha} - E_{g\alpha} \tag{9}$$

$$L_g.\dot{I}_{g\beta} = -R_g.I_{g\beta} + U_{c\beta} - E_{g\beta} \tag{10}$$

$$C_f.\dot{U}_{c\alpha} = I_{f\alpha} - I_{g\alpha} \tag{11}$$

$$C_f.\dot{U}_{c\beta} = I_{f\beta} - I_{g\beta} \tag{12}$$

$$L_f.\dot{I}_{f\alpha} = -R_f.I_{f\alpha} + V_{pv}.\mu_\alpha - U_{c\alpha} \tag{13}$$

$$L_f.\dot{I}_{f\beta} = -R_f.I_{f\beta} + V_{pv}.\mu_\beta - U_{c\beta} \tag{14}$$

$$C_{pv}.\dot{V}_{pv} = I_{pv} - \frac{3}{2}(\mu_a.I_{fa} + \mu_\beta.I_{f\beta}) \tag{15}$$

The (9)-(15) describe the thorough dynamical model of a single-stage three-phase grid-connected PV system, distinguished by its nonlinearity due to the inclusion of terms involving products $V_{pv}.\mu_\alpha$, $V_{pv}.\mu_\beta$, $\mu_\alpha.I_{f\alpha}$ and $\mu_\beta.I_{f\beta}$. The active and reactive power delivered to the grid in the αβ-frame can be expressed as [33]:

$$P_g = \frac{3}{2}(E_{g\alpha}.I_{g\alpha} + E_{g\beta}.I_{g\beta}) \tag{16}$$

$$Q_g = \frac{3}{2}(E_{g\beta}I_{g\alpha} - E_{g\alpha}I_{g\beta}) \tag{17}$$

3. CONTROL SYSTEM DEVELOPMENT

In this section, we will design a nonlinear controller in the αβ reference frame for a single-stage three-phase grid-connected PV system through an LCL-filter. The goal of our controller is to achieve both maximum power point operation despite the climatic changes and to control the reactive power thus to keep the unity power factor on the grid side. The control law must ensure that the active power P_{pv} follows the desired active power P_{pv}^* to achieve MPP operation. In this research, a MPPT algorithm based on the perturb and observe technique is used to generate the reference P_{pv}^*. The control law must also force the grid currents $I_{g\alpha}$ and $I_{g\beta}$ to track the reference currents $I_{g\alpha}^* = k.E_{g\alpha}$ and $I_{g\beta}^* = k.E_{g\beta}$ thus to ensure unity power factor on the grid side. Indeed, by utilizing (16)-(17) this choice implies that:

$$P_g = \frac{3}{2}k.(E_{g\alpha}^2 + E_{g\beta}^2) \text{ and } Q_g = 0 \tag{18}$$

where k is a positive real signal fixing the amplitudes of the grid currents to be defined later.

Assuming that the inverter is lossless and neglecting the power loss on the LCL-filter, the PV power is equal to the active power injected into the grid, thus.

$$P_g = \frac{3}{2}(E_{g\alpha}I_{g\alpha} + E_{g\beta}I_{g\beta}) = P_{pv} \tag{19}$$

Now, considering that both of these objectives are accomplished, from the above equations, we can obtain.

$$k = \frac{2.P_{pv}^*}{3.(E_{g\alpha}^2+E_{g\beta}^2)} \tag{20}$$

Therefore, the reference currents for $I_{g\alpha}$ and $I_{g\beta}$ become:

$$I_{g\alpha}^* = \frac{2.P_{pv}^*.E_{g\alpha}}{3.(E_{g\alpha}^2+E_{g\beta}^2)} \text{ and } I_{g\beta}^* = \frac{2.P_{pv}^*.E_{g\beta}}{3.(E_{g\alpha}^2+E_{g\beta}^2)} \tag{21}$$

3.1. Controller design

This subsection aims to find the control laws, μ_α and μ_β, in such a way that the output currents of the LCL-filter $I_{g\alpha}$ and $I_{g\alpha}$ can track their predefined references $I_{g\alpha}^*$ and $I_{g\alpha}^*$ to achieve both maximum power point (MPP) operation and unity power factor on the grid side simultaneously. To accomplish this, a control strategy is designed in three steps using the backstepping technique.

- Step 1: Stabilization of the subsystem (9)

Let's define the following tracking error:

$$z_1 = L_g(I_{g\alpha} - I_{g\alpha}^*) \tag{22}$$

The time derivative of z_1 is written as (23).

$$\dot{z}_1 = L_g(\dot{I}_{g\alpha} - \dot{I}_{g\alpha}^*) \tag{23}$$

By substituting the value of $\dot{I}_{g\alpha}$ from (9), we can express the dynamics of z_1 as (24).

$$\dot{z}_1 = -R_g I_{g\alpha} + U_{c\alpha} - E_{g\alpha} - L_g\dot{I}_{g\alpha}^* \tag{24}$$

Then, considering the Lyapunov candidate function V_1:

$$V_1 = \frac{1}{2}z_1^2 \tag{25}$$

The time derivative of V_1 is:

$$\dot{V}_1 = z_1\dot{z}_1 \tag{26}$$

Substituting (24) into (26), yields:

$$\dot{V}_1 = z_1.(-R_g I_{g\alpha} + U_{c\alpha} - E_{g\alpha} - L_g \dot{I}^*_{g\alpha}) \quad (27)$$

The choice of $U_{c\alpha}$ as a virtual control input leads to the following stabilizing function, obtained by respecting the Lyapunov candidate function V_1 and its dynamic $\dot{V}_1$, which requires $\dot{V}_1 \leq 0$.

$$U_{c\alpha} = \alpha_0 = -c_1 z_1 + R_g I_{g\alpha} + E_{g\alpha} + L_g \dot{I}^*_{g\alpha} \quad (28)$$

Where c_1 is a positive constant parameter utilized to regulate the system's output response. In fact, this choice implies that:

$$\dot{V}_1 = -c_1.z_1^2 \leq 0 \quad (29)$$

Given that $U_{c\alpha}$ is not the actual control input, we introduce a new error variable:

$$z_2 = C_f(U_{c\alpha} - \alpha_0) \quad (30)$$

Using (24), (26), (28), and (30), the dynamics of tracking error z_1 and Lyapunov candidate function V_1 become:

$$\dot{z}_1 = -c_1 z_1 + \frac{z_2}{C_f} \quad (31)$$

$$\dot{V}_1 = -c_1 z_1^2 + \frac{z_1 z_2}{C_f} \quad (32)$$

- Step 2: Stabilization of the sub-system (9) and (11)

Following the same procedure as in the first step, using (11), the dynamic of tracking error z_2 is written as:

$$\dot{z}_2 = I_{f\alpha} - I_{g\alpha} - C_f \dot{\alpha}_0 \quad (33)$$

Then, considering the augmented Lyapunov candidate function V_2:

$$V_2 = V_1 + \frac{1}{2} z_2^2 \quad (34)$$

Using (32), the dynamic of Lyapunov candidate function V_2 gives:

$$\dot{V}_2 = -c_1 z_1^2 + z_2(\frac{z_1}{C_f} + \dot{z}_2) \quad (35)$$

Substituting (33) into (35), yields:

$$\dot{V}_2 = -c_1 z_1^2 + z_2(\frac{z_1}{C_f} + I_{f\alpha} - I_{g\alpha} - C_f \dot{\alpha}_0) \quad (36)$$

The choice of $I_{f\alpha}$ as a virtual control input leads to the following stabilizing function, obtained by respecting the Lyapunov candidate function V_2 and its dynamic $\dot{V}_2$, which requires $\dot{V}_2 \leq 0$.

$$I_{f\alpha} = \alpha_1 = -c_2 z_2 - \frac{z_1}{C_f} + I_{g\alpha} + C_f \dot{\alpha}_0 \quad (37)$$

where c_2 is a positive constant parameter utilized to regulate the system's output response. In fact, this choice implies that:

$$\dot{V}_2 = -c_1 z_1^2 - c_2 z_2^2 \leq 0 \quad (38)$$

As $I_{f\alpha}$ is not the actual control input, a third error variable z_3 is defined:

$$z_3 = L_f(I_{f\alpha} - \alpha_1) \quad (39)$$

Utilizing in (33), (35), (36), and (39), the dynamics of tracking error z_2 and Lyapunov candidate function V_2 become:

$$\dot{z}_2 = -c_2 z_2 - \frac{z_1}{C_f} + \frac{z_3}{L_f} \tag{40}$$

$$\dot{V}_2 = -c_1 z_1^2 - c_2 z_2^2 + \frac{z_2 z_3}{L_f} \tag{41}$$

- Step 3: Stabilizing of (7), (9), and (11)

In a similar manner to the procedure employed in the initial two steps and utilizing (13), the dynamic of the error variable z_3 can be as:

$$\dot{z}_3 = -R_f I_{f\alpha} + V_{pv}.\mu_\alpha - U_{c\alpha} - L_f \dot{\alpha}_1 \tag{42}$$

Then, considering the augmented Lyapunov candidate function V_3:

$$V_3 = V_2 + \frac{1}{2} z_3^2 \tag{43}$$

Utilizing in (41), the dynamic of the Lyapunov candidate function V_3 is given as

$$\dot{V}_3 = -c_1 z_1^2 - c_2 z_2^2 + z_3 (\frac{z_2}{L_f} + \dot{z}_3) \tag{44}$$

For making V_3 negative definite function, let us take:

$$\dot{z}_3 = -c_3 z_3 - \frac{z_2}{L_f} \tag{45}$$

where c_3 is a positive constant parameter utilized to regulate the system's output response. In fact, this choice implies that:

$$\dot{V}_3 = -c_1 z_1^2 - c_2 z_2^2 - c_3 z_3^2 \leq 0 \tag{46}$$

Combining (42) and (46), the expression of the effective control law μ_α, is given by:

$$\mu_\alpha = \frac{1}{V_{pv}} (-c_3 z_3 - \frac{z_2}{L_f} + R_f I_{f\alpha} + U_{c\alpha} + L_f \dot{\alpha}_1) \tag{47}$$

Remark: The control law for the β-axis can be derived in a similar manner to the α-axis, given that the equations of the system (9-14) exhibit similarity on both axes of the αβ-frame.

Proposition 1: Consider the subsystem, described by model (9), (11) and (13) with the control law (47). In closed loop, the system behavior is described in the error coordinate (z_1, z_2, z_3) by:

$$\begin{bmatrix} \dot{z}_1 \\ \dot{z}_2 \\ \dot{z}_3 \end{bmatrix} = \begin{bmatrix} -c_1 & \frac{1}{C_f} & 0 \\ -\frac{1}{C_f} & -c_2 & \frac{1}{L_f} \\ 0 & -\frac{1}{L_f} & -c_3 \end{bmatrix} \begin{bmatrix} z_1 \\ z_2 \\ z_3 \end{bmatrix} \tag{48}$$

Consequently, the closed loop system is globally asymptotically stable.

4. SIMULATION RESULTS

In this section, the PV system equipped with the designed controller shown in Figure 4 is thoroughly evaluated under various atmospheric conditions. The evaluation is carried out in the presence of the following scenarios: i) Standard atmospheric conditions; ii) Changes of irradiation with standard temperature; and iii) Changes of temperature with standard irradiation. The parameters of the designed controller are listed in Table 5. They were chosen using a 'trial-and-error' search method to ensure their suitability for the system's operation.

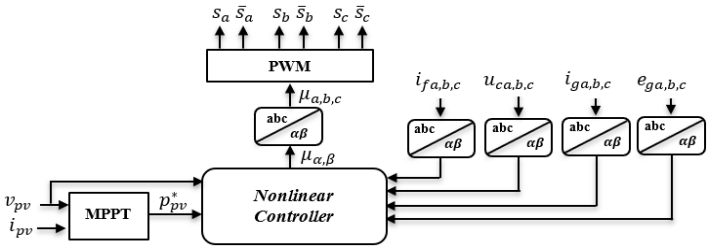

Figure 4. Controller schematic diagram for a single-stage three-phase grid-connected PV system

Table 5. Controller parameters

Parameter	Value
c_1	1.10^{10}
c_2	1.10^4
c_3	1.10^4

4.1. Controller performance under standard atmospheric conditions

In this case, we are considering standard atmospheric conditions i.e. $E = 1000\ W/m^2$ and T=25 °C. Figure 5 depicts the power supplied by the photovoltaic generator and the ideal PV power (MPP1) listed in Table 2. After a brief start-up phase, the PV power stabilizes at an average value of approximately 99607.22 W. It is evident that this value is very close to the ideal power.

Figure 6 shows the current and voltage of the grid. From this figure, it is evident that the grid current is sinusoidal and in phase with the grid voltage. Consequently, the power factor is unity, which aligns with the desired objective. Figure 7 illustrates the harmonic analysis of the grid current and shows an extremely low value of 0.07%, confirming the quality of the current injected into the grid.

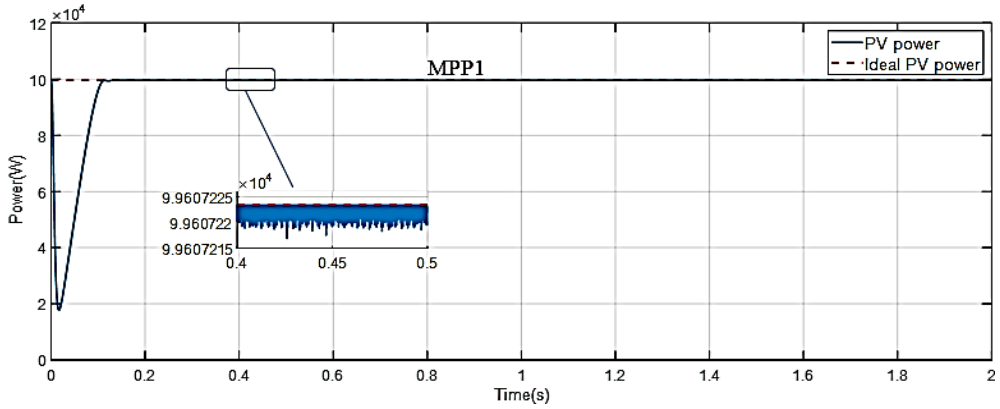

Figure 5. PV power and ideal PV power

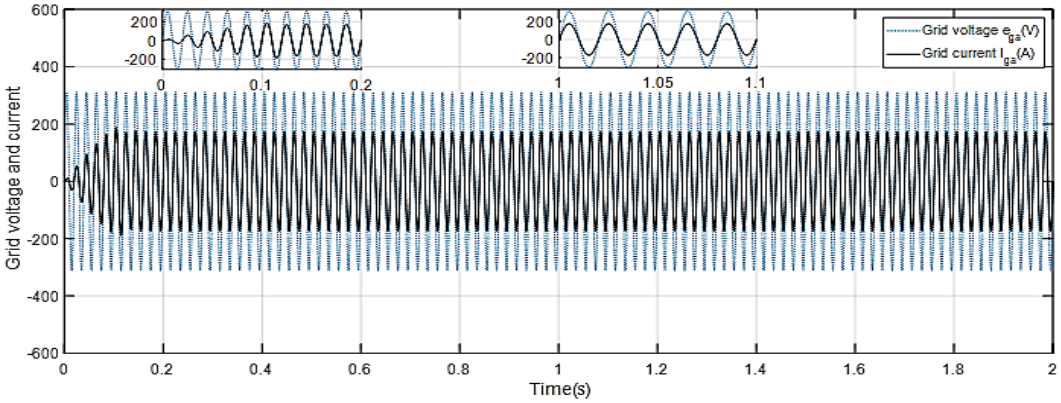

Figure 6. Grid voltage and current at standard atmospheric conditions

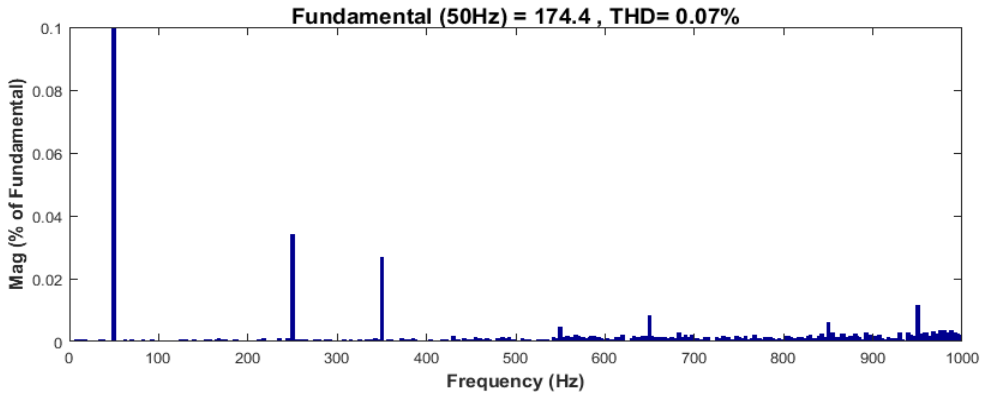

Figure 7. Total harmonic distortion of grid current at standard atmospheric conditions

4.2. Controller performance under changes of irradiation

In general, solar irradiance fluctuates throughout the day, which affects the maximum power point of the photovoltaic generator, as shown in Table 2. To evaluate the controller's performance under varying irradiance conditions, the system is subjected to the solar irradiance profile shown in Figure 8. Throughout the simulation, the temperature is kept constant at 25 °C.

Figure 9 depicts the trajectory of the power supplied by the photovoltaic generator. It can be seen that after a short start-up phase, the PV system operates at its MPP, demonstrating its ability to adapt to changing solar irradiance conditions. Figure 10 demonstrates that the grid current and voltage are in phase all the time, regardless of the changes in irradiation. This confirms the successful achievement of UPF objective. In Figure 11, the total harmonic distortion (THD) of the grid current is shown at an irradiance of $E = 800\ W/m^2$. The THD value is approximately 0.07%.

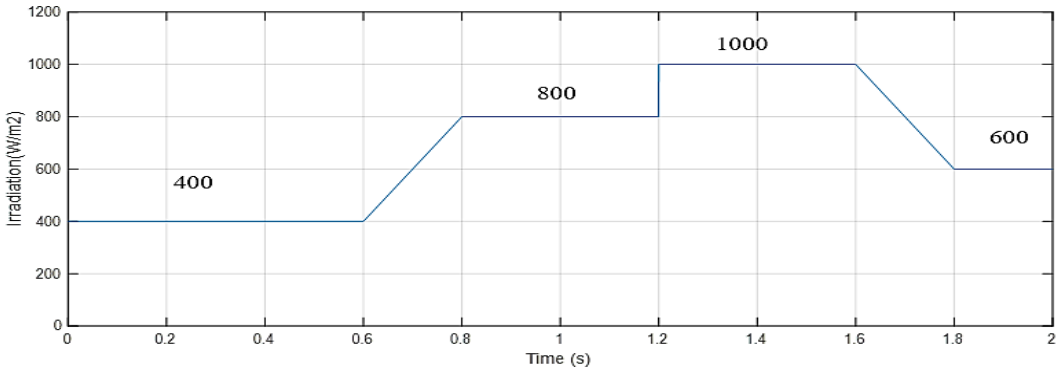

Figure 8. Solar irradiance profile

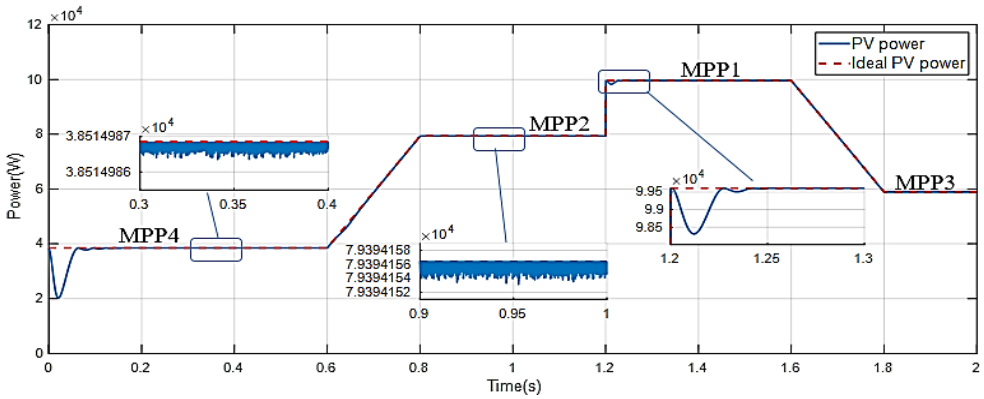

Figure 9. PV power and ideal PV power

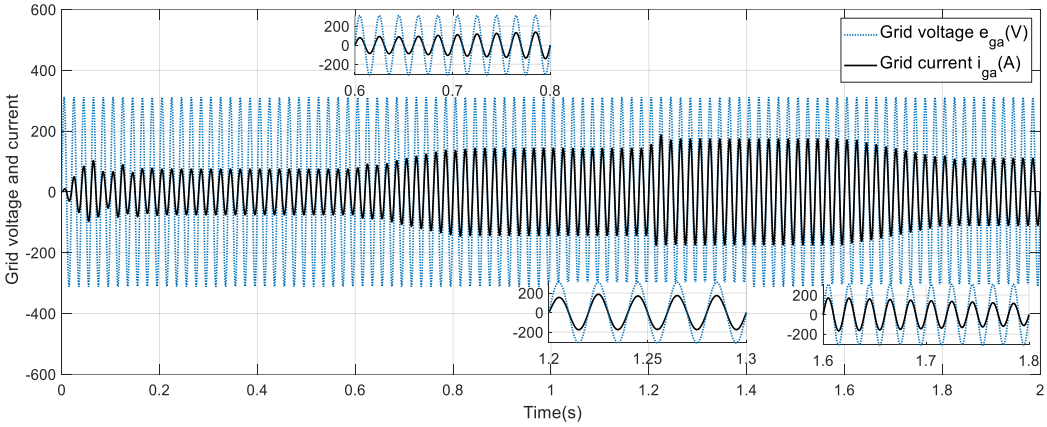

Figure 10. Grid voltage and current under changes of irradiation

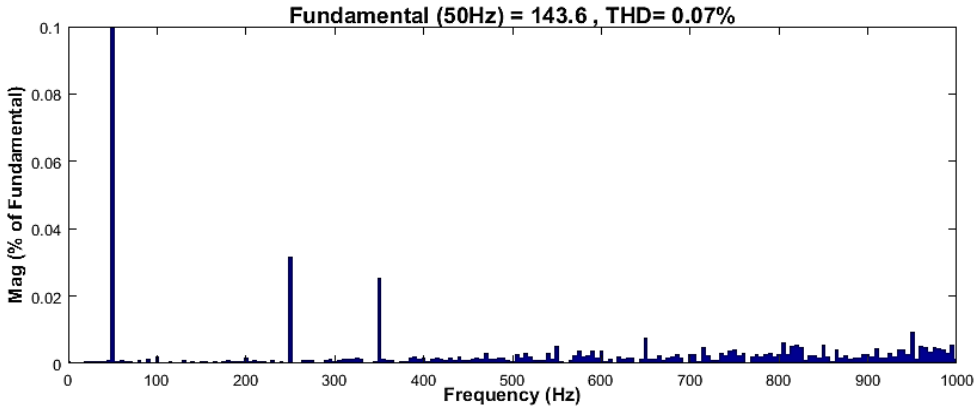

Figure 11. Total harmonic distortion of grid current at E = 800 W/m^2

4.3. Controller performance under changes of temperature

In this case, we evaluated the performance of the designed controller under varying temperature conditions by using the temperature profile depicted in Figure 12. Throughout the simulation, the solar irradiation remained constant at E = 1000 W/m^2. Figure 13 shows the trajectory of the power provided by the photovoltaic generator. from this figure, it can be seen that after a short start-up phase, the PV system operates at its MPP, regardless of temperature changes. Figure 14 demonstrates that the grid current and voltage are always in phase, which confirms the achievement of the UPF objective. In Figure 15, the THD of the grid current is shown at T=15 °C, indicating a low value of 0.07%.

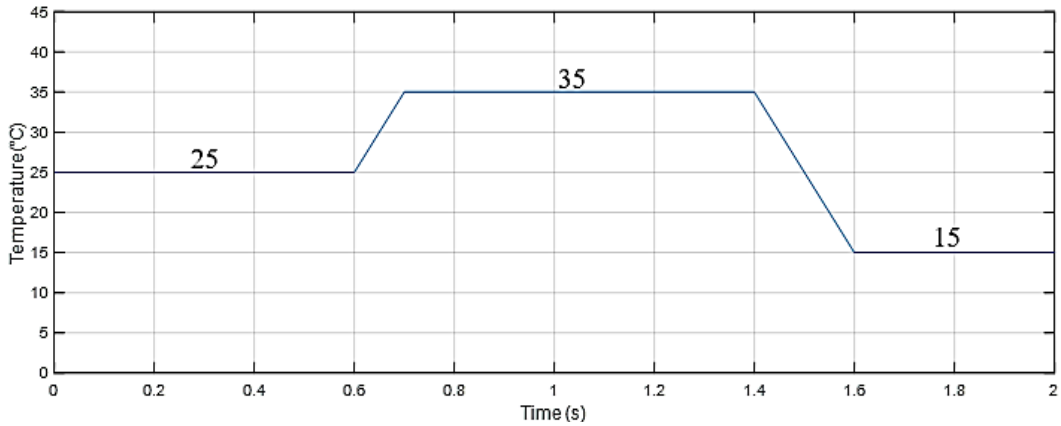

Figure 12. Temperature profile

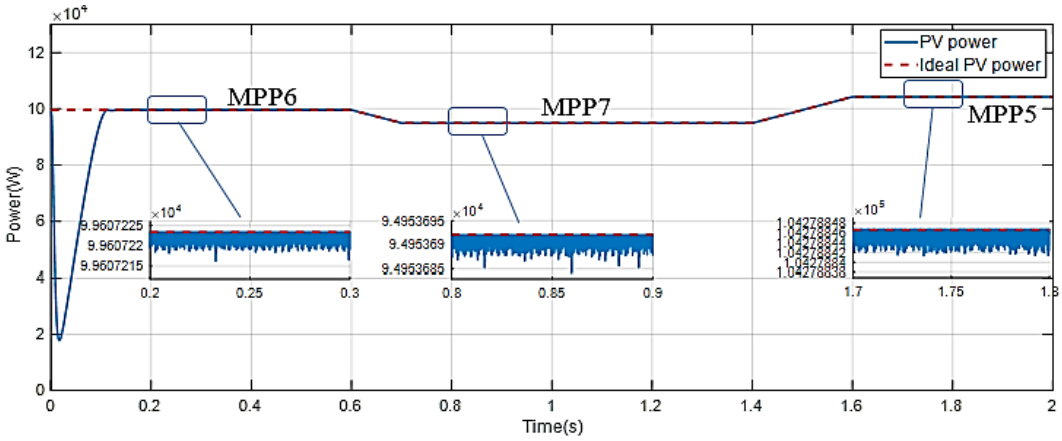

Figure 13. PV power and ideal PV power

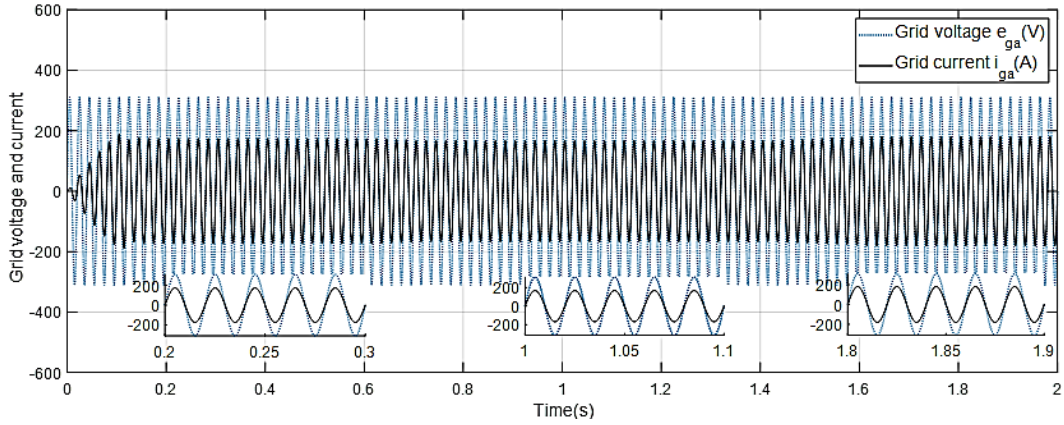

Figure 14. Grid voltage and current under changes of temperature

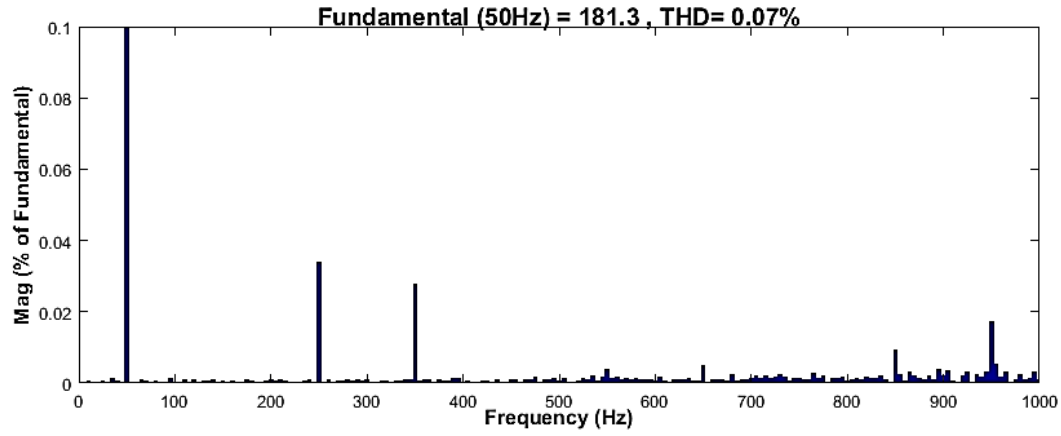

Figure 15. Total harmonic distortion of grid current at T=15 °C

5. CONCLUSION

In this paper, we have developed a mathematical model in the $\alpha\beta$ reference frame for a single-stage three-phase grid-connected PV system with an LCL-filter. This model serves as the basis for designing a nonlinear backstepping controller, which aims to achieve maximum power point operation under various atmospheric conditions while also maintaining control of reactive power to ensure unity power factor on the grid side. The stability of the entire system has been rigorously validated using Lyapunov tools. Through comprehensive evaluations of tracking performance, stability, and system dynamics, we have demonstrated

that the proposed scheme with the nonlinear controller yields significant improvements in power quality, notably reducing total harmonic distortion (THD) values.

REFERENCES

[1] Y. Chaibi, A. Allouhi, M. Salhi, and A. El-jouni, "Annual performance analysis of different maximum power point tracking techniques used in photovoltaic systems," *Protection and Control of Modern Power Systems*, vol. 4, no. 1, 2019, doi: 10.1186/s41601-019-0129-1.

[2] A. O. Baba, G. Liu, and X. Chen, "Classification and evaluation review of maximum power point tracking methods," *Sustainable Futures*, vol. 2, 2020, doi: 10.1016/j.sftr.2020.100020.

[3] A. A. Abdulrazzaq and A. H. Ali, "Efficiency performances of two MPPT algorithms for PV system with different solar panels irradiances," *International Journal of Power Electronics and Drive Systems*, vol. 9, no. 4, pp. 1755–1764, 2018, doi: 10.11591/ijpeds.v9.i4.pp1755-1764.

[4] T. Abderrahim, T. Abdelwahed, and M. Radouane, "Improved strategy of an MPPT based on the sliding mode control for a PV system," *International Journal of Electrical and Computer Engineering*, vol. 10, no. 3, pp. 3074–3085, 2020, doi: 10.11591/ijece.v10i3.pp3074-3085.

[5] A. S. Mahdi, A. K. Mahamad, S. Saon, T. Tuwoso, H. Elmunsyah, and S. W. Mudjanarko, "Maximum power point tracking using perturb and observe, fuzzy logic, and ANFIS," *SN Applied Sciences*, vol. 2, no. 1, 2020, doi: 10.1007/s42452-019-1886-1.

[6] J. S. Kumari and C. Saibabu, "Maximum power point tracking algorithms for grid-connected photovoltaic energy conversion system," *International Journal of Power Electronics and Drive Systems*, vol. 3, no. 4, pp. 424–437, 2013, doi: 10.11591/ijpeds.v3i4.4313.

[7] R. Kahani, M. Jamil, and M. T. Iqbal, "An improved perturb and observed maximum power point tracking algorithm for photovoltaic power systems," *Journal of Modern Power Systems and Clean Energy*, vol. 11, no. 4, pp. 1165–1175, 2023, doi: 10.35833/MPCE.2022.000245.

[8] J. J. Nedumgatt, K. B. Jayakrishnan, S. Umashankar, D. Vijayakumar, and D. P. Kothari, "Perturb and observe MPPT algorithm for solar PV systems-modeling and simulation," 2011, doi: 10.1109/INDCON.2011.6139513.

[9] J. Ahmed and Z. Salam, "An improved perturb and observe (P&O) maximum power point tracking (MPPT) algorithm for higher efficiency," *Applied Energy*, vol. 150, pp. 97–108, 2015, doi: 10.1016/j.apenergy.2015.04.006.

[10] H. Attia and S. Ulusoy, "A new perturb and observe MPPT algorithm based on two steps variable voltage control," *International Journal of Power Electronics and Drive Systems*, vol. 12, no. 4, pp. 2201–2208, 2021, doi: 10.11591/ijpeds.v12.i4.pp2201-2208.

[11] M. Aourir, A. Abouloifa, I. Lachkar, C. Aouadi, F. Giri, and J. M. Guerrero, "Nonlinear control and stability analysis of single stage grid-connected photovoltaic systems," *International Journal of Electrical Power and Energy Systems*, vol. 115, 2020, doi: 10.1016/j.ijepes.2019.105439.

[12] K. R. Reddy, V. N. Reddy, and M. V. Kumar, "A sliding mode controller approach for three phase single stage seven level multilevel inverter for grid connected photovoltaic system," *International Journal of Renewable Energy Research*, vol. 10, no. 4, pp. 1674–1684, 2020, doi: 10.20508/ijrer.v10i4.11289.g8052.

[13] D. P. Mishra, K. K. Rout, S. Mishra, M. Nivas, R. K. P. R. Naidu, and S. R. Salkuti, "Power quality enhancement of grid-connected PV system," *International Journal of Power Electronics and Drive Systems*, vol. 14, no. 1, pp. 369–377, 2023, doi: 10.11591/ijpeds.v14.i1.pp369-377.

[14] S. Naddami and N. Ababssi, "Power quality optimization using a novel backstepping control of a three-phase grid-connected photovoltaic systems," *International Journal of Electrical and Computer Engineering*, vol. 13, no. 3, pp. 2517–2528, 2023, doi: 10.11591/ijece.v13i3.pp2517-2528.

[15] N. Altin, S. Ozdemir, H. Komurcugil, I. Sefa, and S. Biricik, "Two-stage grid-connected inverter for PV systems," in *Proceedings - 2018 IEEE 12th International Conference on Compatibility, Power Electronics and Power Engineering, CPE-POWERENG 2018*, 2018, pp. 1–6, doi: 10.1109/CPE.2018.8372540.

[16] C. L. Trujillo, F. Santamaría, and E. E. Gaona, "Modeling and testing of two-stage grid-connected photovoltaic micro-inverters," *Renewable Energy*, vol. 99, pp. 533–542, 2016, doi: 10.1016/j.renene.2016.07.011.

[17] A. Yahya, H. El Fadil, F. Giri, and H. Erguig, "Advanced control of three-phase grid connected PV generator," in *Proceedings of 2014 International Renewable and Sustainable Energy Conference, IRSEC 2014*, 2014, pp. 753–758, doi: 10.1109/IRSEC.2014.7059763.

[18] M. El malah, A. Ba-Razzouk, M. Guisser, E. Abdelmounim, and M. Madark, "Backstepping based power control of a three-phase single-stage grid-connected PV system," *International Journal of Electrical and Computer Engineering*, vol. 9, no. 6, pp. 4738–4748, 2019, doi: 10.11591/ijece.v9i6.pp4738-4748.

[19] T. K. Roy, M. A. Mahmud, M. J. Hossain, and A. M. T. Oo, "Nonlinear backstepping controller design for sharing active and reactive power in three-phase grid-connected photovoltaic systems," 2015, doi: 10.1109/AUPEC.2015.7324866.

[20] P. R. Rivera, M. L. McIntyre, M. Mohebbi, and J. Latham, "Nonlinear control for single-stage single-phase grid-connected photovoltaic systems," *2017 IEEE 18th Workshop on Control and Modeling for Power Electronics, COMPEL 2017*, 2017, doi: 10.1109/COMPEL.2017.8013366.

[21] M. D. and V. Sankaranarayanan, "A novel nonlinear sliding mode controller for a single stage grid-connected photovoltaic system," *ISA Transactions*, vol. 107, pp. 329–339, 2020, doi: 10.1016/j.isatra.2020.07.021.

[22] K. R. Reddy, V. N. Reddy, and M. V. Kumar, "Control of single stage grid tied photovoltaic inverter using incremental conductance method," *International Journal of Power Electronics and Drive Systems*, vol. 9, no. 4, pp. 1702–1708, 2018, doi: 10.11591/ijpeds.v9.i4.pp1702-1708.

[23] M. Dursun and M. K. Dosoglu, "LCL filter design for grid connected three-phase inverter," *ISMSIT 2018 - 2nd International Symposium on Multidisciplinary Studies and Innovative Technologies, Proceedings*, 2018, doi: 10.1109/ISMSIT.2018.8567054.

[24] A. K. Sahoo, A. Shahani, K. Basu, and N. Mohan, "LCL filter design for grid-connected inverters by analytical estimation of PWM ripple voltage," in *Conference Proceedings - IEEE Applied Power Electronics Conference and Exposition - APEC*, 2014, pp. 1281–1286, doi: 10.1109/APEC.2014.6803471.

[25] N. A. Sabran, C. L. Toh, and C. W. Tan, "LCL-filter design and analysis for PWM recuperating system used in DC traction power substation," *International Journal of Power Electronics and Drive Systems*, vol. 13, no. 4, pp. 2244–2254, 2022, doi: 10.11591/ijpeds.v13.i4.pp2244-2254.

[26] Y. J. Kim and H. Kim, "Optimal design of LCL filter in grid-connected inverters," *IET Power Electronics*, vol. 12, no. 7, pp. 1774–1782, 2019, doi: 10.1049/iet-pel.2018.5518.

[27] C. Gurrola-Corral, J. Segundo, M. Esparza, and R. Cruz, "Optimal LCL-filter design method for grid-connected renewable energy sources," *International Journal of Electrical Power & Energy Systems*, vol. 120, p. 105998, Sep. 2020, doi: 10.1016/j.ijepes.2020.105998.
[28] M. B. Saïd-Romdhane, M. W. Naouar, I. S. Belkhodja, and E. Monmasson, "Simple and systematic LCL filter design for three-phase grid-connected power converters," *Mathematics and Computers in Simulation*, vol. 130, pp. 181–193, 2016, doi: 10.1016/j.matcom.2015.09.011.
[29] C. Poongothai and K. Vasudevan, "Design of LCL filter for grid-interfaced PV system based on cost minimization," *IEEE Transactions on Industry Applications*, vol. 55, no. 1, pp. 584–592, 2019, doi: 10.1109/TIA.2018.2865723.
[30] W. Hong and G. Tao, "An adaptive control scheme for three-phase grid-connected inverters in photovoltaic power generation systems," in *Proceedings of the American Control Conference*, 2018, vol. 2018-June, pp. 899–904, doi: 10.23919/ACC.2018.8430967.
[31] W. Hong, G. Tao, and H. Wang, "An output feedback MRAC Scheme for three-phase grid-connected inverters in photovoltaic power generation systems," in *Proceedings of the IEEE Conference on Decision and Control*, 2018, vol. 2018-Decem, pp. 3439–3444, doi: 10.1109/CDC.2018.8619111.
[32] P. T. Krein, J. Bentsman, R. M. Bass, and B. L. Lesieutre, "On the use of averaging for the analysis of power electronic systems," *IEEE Transactions on Power Electronics*, vol. 5, no. 2, pp. 182–190, 1990, doi: 10.1109/63.53155.
[33] C. J. O'Rourke, M. M. Qasim, M. R. Overlin, and J. L. Kirtley, "A geometric interpretation of reference frames and transformations: Dq0, clarke, and park," *IEEE Transactions on Energy Conversion*, vol. 34, no. 4, pp. 2070–2083, 2019, doi: 10.1109/TEC.2019.2941175.

BIOGRAPHIES OF AUTHORS

Zakariae El Madani received his B.S. degree in Electrical Engineering and Industrial Computing, and master's degree in Electrical Engineering from ENSAM, Mohammed V University, Rabat, Morocco, as well as agrégation degree in Electrical Engineering, in 2014, 2016 and 2019 respectively. He is currently pursuing the Ph.D. degree in Electrical Engineering at Higher School of technology, Meknes, Morocco. He can be contacted at email: zakariae.elmadani@gmail.com.

Abdelhafid Yahya obtained his bachelor's degree in Electrotechnical, agrégation degree in Electrical Engineering, master's degree in Electronics and Telecommunication from the University Abdelmalek Saadi of Tetouan Morocco and his doctorate in Electrical Engineering in 1997, 2010, 2012 and 2019 respectively. He is also an assistant professor at the Department of Electrical Engineering, Higher School of technology, Meknes, Morocco. His research interests include new energy technologies, simulation methods, power systems dynamics and control, power electronics modeling and design, renewable energy resources, and the application of energy storage in power systems. He can be contacted at email: yaabha2@gmail.com.

Zakaria El Malki is professor in The Higher School of Technology (ESTM) University Moulay Ismail of Meknes, Morocco. He has received his Ph.D. in Physical and Electrical Engineering in 2011 from Faculty of Sciences of Meknes, Affiliated to Moulay Ismaïl University in Morocco. He pursued his research in the Department of Electrical Engineering, Higher School of technology, Meknes. His major research interests include new energy technologies, simulation methods, power systems dynamics and control, renewable energy resources and Molecular Modeling of the optoelectronic properties and vibrational spectroscopy of organic molecules and polymers and characterization of new pi-conjugated nanostructures for the realization of organic solar cells, OLEDs, and OTFTs applications. He can be contacted at email: zelmalki@yahoo.fr.